

Ionization wave propagation on a micro cavity plasma array

Alexander Wollny,^{1,a)} Torben Hemke,¹ Markus Gebhardt,¹ Ralf Peter Brinkmann,¹ Henrik Boettner,² Jörg Winter,² Volker Schulz-von der Gathen,² Zhongmin Xiong,³ Mark J. Kushner,³ and Thomas Mussenbrock¹

¹*Institute of Theoretical Electrical Engineering, Ruhr University Bochum, D-44780 Bochum, Germany*

²*Institute for Experimental Physics II, Ruhr University Bochum, D-44780 Bochum, Germany*

³*Department of Electrical Engineering and Computer Science, University of Michigan, 1301 Beal Ave., Ann Arbor, Michigan 48109, USA*

(Received 29 April 2011; accepted 19 September 2011; published online 6 October 2011)

Microcavity plasma arrays of inverse pyramidal cavities fabricated on p-Si wafers act as localized dielectric barrier discharges. When operated at atmospheric pressure in argon and excited with high voltage at 10 kHz, a strong interaction between individual cavities is observed leading to wave-like optical emission propagating along the surface of the array. This phenomenon is numerically investigated. The computed ionization wave propagates with a speed of 5 km/s, which agrees well with experiments. The wave propagation is due to the sequential drift of electrons followed by drift of ions between cavities seeded by photoemission of electrons by the plasma in adjacent cavities. © 2011 American Institute of Physics. [doi:10.1063/1.3647978]

Atmospheric pressure microplasmas have gained increasing attention since the early work on microhollow cathode discharges by Schoenbach *et al.*¹ Although they are highly collisional, microplasmas show strong non-equilibrium behavior.² Electrons are hot (up to a few eV) while ions and the neutral gas are cold (about room temperature in most cases, though temperatures of many hundreds centigrade occur at high power loading). Microplasmas are characterized by high electron densities (up to a few 10^{17} cm⁻³) and high power densities (up to many hundreds kW/cm³). Due to these unique properties, microplasmas have found widespread use in technological and biomedical applications,^{3–6} such as surface treatment, sterilization, and lighting. At the same time, microplasmas continue to show unexpected phenomena and are therefore scientifically interesting. For example, arrays of microplasmas having thousands of individual microdischarges have been fabricated as efficient lighting sources.⁷ When excited by AC voltages, the initiation of optical emission from such arrays has shown wave-like phenomena, propagating across the array at speeds of a few kilometers per second. In this paper, we discuss results from experimental and computational investigations of this wave-like propagation of optical emission.

The microcavity array we investigated, developed by Eden *et al.*,⁷ has individual inverse pyramidal cavities fabricated on p-Si wafers (see Fig. 1), combined with a nickel grid as a counter electrode and dielectric coatings. Each cavity—in essence a microscopic dielectric barrier discharge (DBD)—has a base opening of 50×50 μm and a depth of 35 μm . The separation of the individual cavities is 50 μm . The entire array consists of 50 by 50 microplasmas. When operated with a sawtooth voltage of about 10 kHz in atmospheric pressure argon, the array emits a bright glow in the visible wavelength range, which visually appears homogeneous over the entire array. However, spatially and temporally

resolved emission spectroscopy shows that wave-like structures (see Fig. 2) propagate across the array, indicating that the individual microdischarges strongly interact with each other.^{8,9}

The simulation was performed using the computer modeling platform *nonPDPSIM*, described in detail in Refs. 10–12 and briefly discussed here. Poisson's equation for the electrostatic potential is self-consistently coupled with drift-diffusion equations for the transport of charged species and the surface charge balance equation. The set of equations is simultaneously integrated in time using an implicit Newton iteration technique. This integration step is followed by an implicit update of the electron temperature by solving the electron energy equation. To capture the non-Maxwellian behavior of the electrons, the electron transport coefficients and rate coefficients are obtained by solving the zero-dimensional Boltzmann's equation for the electron energy distribution. A Monte Carlo simulation is used to track the trajectories of sheath accelerated secondary electrons. The transport of photons is treated by means of a Green's function propagator. The discharge is sustained in argon at atmospheric pressure. The species in the model are electrons, Ar(3s), Ar(4s), Ar(4p), Ar⁺, Ar₂^{*}, and Ar₂⁺. The photon transport we tracked in the model is dimer radiation from Ar₂^{*}. In

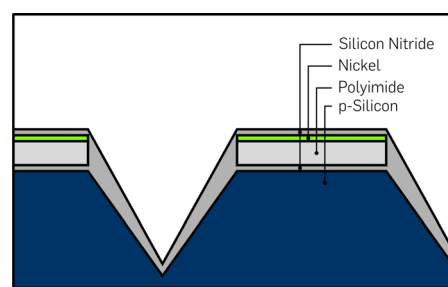


FIG. 1. (Color online) Schematics of the modeled micro cavity. p-silicon wafer: anode, $\phi = 0$ V; silicon nitride and polyimide: dielectrics; embedded nickel grid: cathode, $\phi = -500$ V.

^{a)}Author to whom correspondence should be addressed. Electronic mail: wollny@tet.rub.de.

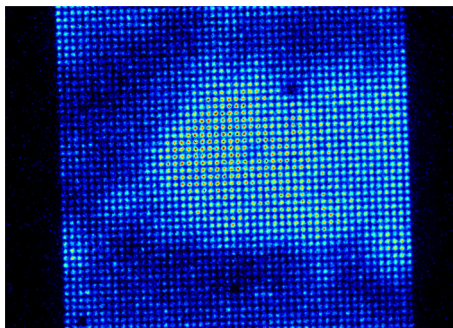


FIG. 2. (Color online) Experimental result from phase resolved optical emission spectroscopy of the microplasma array as registered with an intensified charge-coupled device (ICCD) camera (false colors) for a gate interval of 100 ns and spectrally integrated ($p = 10^5$ Pa Ar, $U_{pp} = 830$ V, $f_{ac} = 20$ kHz). Image taken at $V(t) = -400$ V applied to Ni-grid.

the absence of impurities and large densities of excited states, the plasma is optically thin at 126 nm. The reaction mechanism is summarized in Ref. 13.

The simulation addresses a sub-system of the microcavity array over a time interval of 50 ns. The geometry is

two-dimensional and consists of three neighboring cavities, which appear in the model as slits. The entire computational domain is 1 mm tall by 1.5 mm wide, with boundaries that are electrically grounded. The conductivity of the wafer in contact with the boundary is $0.17 \Omega^{-1} \text{ cm}^{-1}$. The secondary electron emission coefficient by ions is 0.15 on all surfaces. A photoelectron emission coefficient of 0.05 is assumed on the dielectric surface. The step function DC potential of -500 V is applied to the embedded nickel electrode grid.

The initial plasma density is a Gaussian shaped spot of plasma $10 \mu\text{m}$ wide and $5 \times 10^{10} \text{ cm}^{-3}$ in magnitude at the left vertex of the left cavity. The resulting electron density as a function of time is shown in Fig. 3. Ions accelerated by the negative potential of the nickel grid drift towards the vertex of the cavity and initiate secondary electron emission. The secondary electrons are accelerated into the cavity, generating ions and electrons. The ionization rate peaks at the vertices at about $5 \times 10^{24} \text{ cm}^{-3} \text{ s}^{-1}$ with an electron temperature of 8 eV and then spreads on the top dielectric, similar to a conventional DBD. Meanwhile, photons produced by relaxation of Ar_2^* lead to photoelectron emission on the dielectric surfaces, mainly at the right vertex of the neighboring cavity.

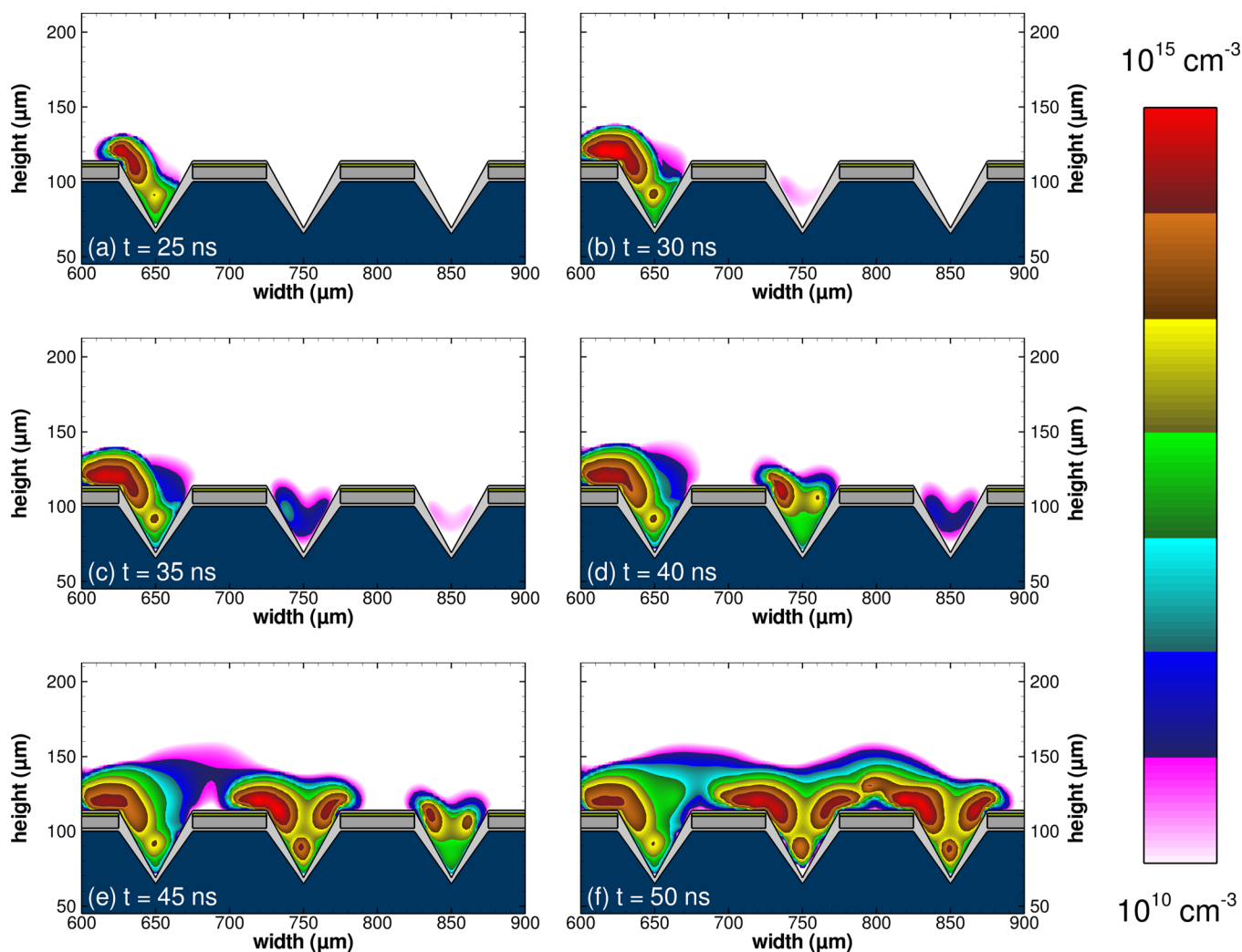


FIG. 3. (Color online) Temporal evolution of the electron density distribution in units of cm^{-3} on logarithmic scale. (a)-(f) The ignition of the three cavities starting at 25 ns in time steps of $\Delta t = 5$ ns. The width and separation of a single cavity is $50 \mu\text{m}$, the overall depth is $45 \mu\text{m}$. The simulation is performed for Ar as a working gas at atmospheric pressure, a driving DC voltage of -500 V applied to the embedded Ni-grid.

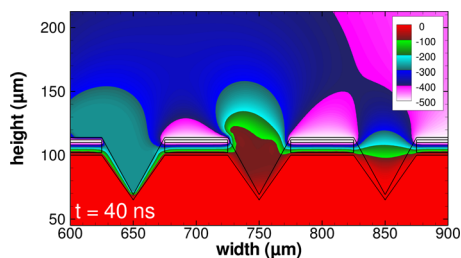


FIG. 4. (Color online) Simulated potential at $t = 80$ ns. Left hand cavity is ignited whereas right hand cavity shows vacuum potential. Centered cavity is in the stage of transition from Townsend mode to glow mode.

At $t = 25$ ns, a sufficiently large electron density of about 10^{15} cm^{-3} is reached in the left cavity, which shields the potential from the interior of the left cavity and turns the discharge from a Townsend mode to a glow mode. The quasineutral region fills the left cavity and spreads over its edges, charging the top dielectric. 5 ns after the left cavity is ignited, an electron density larger than 10^{10} cm^{-3} is produced in the middle cavity initiated by avalanching of photo-generated electrons, and another 5 ns later in the right cavity. Both cavities undergo a transition from a Townsend mode to glow mode 10 ns after the initial electron density is generated (Figs. 3(d) and 3(e)). In all three cavities, a quasineutral region develops. These individual plasmas connect after their expansion out of the cavities, as shown in Fig. 3(f). The electron density peaks in the head of the avalanche with $n_e = 1.5 \times 10^{16}$ cm^{-3} . Within the cavities, the electron density exceeds 10^{15} cm^{-3} leading to a Debye length $\lambda_D < 1$ μm . During the ignition, the electron temperature reaches 5 eV within the cavities, but decays rapidly. The observed densities agree with values expected for this kind of discharge.³

The electric potential is plotted at $t = 40$ ns in Fig. 4 and shows the three phases of the discharge development. The potential in the right cavity is essentially the vacuum potential—there is little space charge to influence the electrical field. The left cavity in contrast contains a quasineutral plasma with the plasma being nearly equipotential. The majority of the potential is dropped over the dielectrics which cover the anode and the cathode, as one expects for a dielectric barrier discharge. The electron avalanche within the center cavity produces an equipotential channel which merges with that of the left cavity and indicates the transition from a Townsend mode to a glow mode discharge.

Taking the time between the ignition of the left and the right cavity one finds an effective ionization wave propagation speed of about 5 km/s which agrees very well with the measured propagation speed of 5 to 10 km/s. In the absence of photoelectron emission, the propagation speed is about 1 km/s. Although not all effects are addressed in the simulation, the ionization wave is well described. Other effects of importance are surface charges which were accumulated in a previous half cycle and a second ionization wave after a further increase of the voltage. Surface charges accumulated during a previous half cycle with an inverse voltage result in an enhancement of the electrical field and reduce the breakdown voltage. Both are a matter of ongoing research. To summarize, the observed ionization wave is driven by photoelectrons produced by photons emitted in neighboring cavities. This electron source initiates an avalanche in the cavity and provides further photons to sustain the ionization wave propagation.

The authors gratefully acknowledge financial support by the Deutsche Forschungsgemeinschaft in the frame of Research Group 1123 *Physics of Microplasmas*, the *Ruhr University Research School* as well as the *United States Department of Energy Office of Fusion Energy Sciences*.

¹K. H. Schoenbach, R. Verhappen, T. Tessnow, F. E. Peterkin, and W. W. Byszewski, *Appl. Phys. Lett.* **68**, 13 (1996).

²C. Penache, M. Miclea, A. Bräuning-Demian, O. Hohn, S. Schössler, T. Jahnke, K. Niemax, and K. Schmidt-Böcking, *Plasma Sources Sci. Technol.* **11**, 476 (2002).

³K. H. Becker, K. H. Schoenbach, and J. G. Eden, *J. Phys. D: Appl. Phys.* **39**, R55 (2006).

⁴M. G. Kong, G. Kroesen, G. E. Morfill, T. Nosenko, T. Shimizu, J. van Dijk, and J. L. Zimmermann, *New. J. Phys.* **11**, 115012 (2009).

⁵K. H. Becker, H. Kersten, J. Hopwood, and J. L. Lopez, *Eur. Phys. J. D* **60**, 437 (2010).

⁶H. W. Lee, G. Y. Park, Y. S. Seo, Y. H. Im, S. B. Shim, and H. J. Lee, *J. Phys. D: Appl. Phys.* **44**, 053001 (2011).

⁷J. G. Eden, S.-J. Park, N. P. Ostrom, and K.-F. Chen, *J. Phys. D: Appl. Phys.* **38**, 1644 (2005).

⁸J. Waskoenig, D. O'Connell, V. Schulz-von der Gathen, J. Winter, S.-J. Park, and J. G. Eden, *Appl. Phys. Lett.* **92**, 101503 (2008).

⁹H. Boettner, J. Waskoenig, D. O'Connell, T. L. Kim, P. A. Tcherchian, J. Winter, and V. Schulz-von der Gathen, *J. Phys. D: Appl. Phys.* **43**, 124010 (2010).

¹⁰M. J. Kushner, *J. Appl. Phys.* **95**, 846 (2004).

¹¹N. Y. Babaeva, R. Arakoni, and M. J. Kushner, *J. Appl. Phys.* **101**, 123306 (2007).

¹²N. Y. Babaeva and M. J. Kushner, *Plasma Sources Sci. Technol.* **18**, 035009 (2009).

¹³A. N. Bhoj and M. J. Kushner, *J. Phys. D: Appl. Phys.* **37**, 2510 (2004).